Electronic, optical, and thermoelectric properties of $Fe_{2+x}V_{1-x}Al$

D. P. Rai, Sandeep, A. Shankar, R. Khenata, A. H. Reshak, C. E. Ekuma, R. K. Thapa, and San-Huang Ke

Citation: AIP Advances **7**, 045118 (2017); doi: 10.1063/1.4982671
View online: http://dx.doi.org/10.1063/1.4982671
View Table of Contents: http://aip.scitation.org/toc/adv/7/4
Published by the American Institute of Physics

Electronic, optical, and thermoelectric properties of $Fe_{2+x}V_{1-x}Al$

D. P. Rai,[1,a] Sandeep,[2] A. Shankar,[3] R. Khenata,[4] A. H. Reshak,[5,6] C. E. Ekuma,[7,b] R. K. Thapa,[2] and San-Huang Ke[8,c]
[1]*Department of Physics, Pachhunga University College, Aizawl 796001, India*
[2]*Department of Physics, Mizoram University, Aizawl 796009, India*
[3]*Department of Physics, University of North Bengal, Darjeeling 734013, India*
[4]*Laboratoire de Physique Quantique de la Matiére et de Modélisation Mathmatique, Universit de Mascara, Mascara 29000, Algeria*
[5]*New Technologies-Research Centre, University of West Bohemia, Univerzitni 8, 306 14 Pilsen, Czech Republic*
[6]*School of Material Engineering, University Malaysia Perlis, 01007 Kangar, Perlis, Malaysia*
[7]*Department of Physics, Computational Material Physics Group, University of Port Harcourt, PMB, 51001 Rivers, Nigeria*
[8]*MOE Key Laboratory of Microstructured Materials, School of Physics Science and Engineering, Tongji University, 1239 Siping Rd., Shanghai 200092, China*

(Received 25 February 2017; accepted 3 April 2017; published online 24 April 2017)

We report the electronic, optical, and thermoelectric properties of full-Heusler alloy Fe_2VAl with Fe antisite doping ($Fe_{2+x}V_{1-x}Al$) as obtained from the first-principles Tran-Blaha modified Becke-Johnson potential. The results are discussed in relation to the available experimental data and show good agreements for the band gap, magnetic moment, and optical spectra. Exploring our transport data for thermoelectric applicability suggest that $Fe_{2+x}V_{1-x}Al$ is a good candidate with a high figure of merit (ZT) 0.75 (0.65) for $x = 0.25$ (0.50) at room temperature. [http://dx.doi.org/10.1063/1.4982671]

I. INTRODUCTION

Heusler-alloys[1–5] exhibit a wide range of emerging optoelectronic and magnetic properties not limited to high spin polarization and magnetic moment, thermoelectric capabilities, and shape memory.[6–12] Atomistic characterization of the different properties is ascribed to e.g., crystal field splitting, electron correlation, and the d bandwidth. Of particular interest in the Heusler-alloys is the Fe-based family, e.g., Fe_2VAl where Fe antisite can induce emerging phenomena, e.g., a para-to-ferromagnetic phase transition.[13,14] Rather high Curie temperatures ~840 (1100) K has been reported for Fe_3Si (Co_2FeSi).[15,16] Recent studies have also investigated Fe-based Heusler compounds for thermoelectric applications with a figure of merit (ZT) ~ 0.21 for $Fe_2VTa_xAl_{1-x}$ and $Fe_2V_{1-x}W_xAl$ (x=0.05-0.10) at ≈ 400-500 K.[17,18] A high power factor in Fe_2VAl (though its ZT value is not available yet) is a signature of a potential candidate for thermoelectric power generator.[19]

Even at the promising prospect of Fe_2VAl as a thermoelectric material, its device applications has been hindered by the poor figure of merit $ZT = \sigma S^2 T/\kappa$ (σ is electrical conductivity, S is the Seebeck coefficient, and κ is thermal conductivity) and divergent interpretations of the optoelectronic properties. The transport data of Nishino *et al.*[20] showed that Fe_2VAl is on the verge of magnetic ordering with a semiconductor-like behavior in both the spin channels in spite of a clear Fermi cutoff as revealed in their photoemission spectra. The reflectivity data of Lue *et al*[21] showed a

[a]E-mail: dibyaprakashrai@gmail.com
[b]E-mail: cekuma1@gmail.com
[c]E-mail: shke@tongji.edu.cn

band gap of 0.10 eV while from nuclear magnetic resonance (NMR) measurement, it was ~0.2 eV. Several band structure calculations, however, reported pseudogap at the Fermi level, a fingerprint of a non-magnetic semimetal.[13,22–24] The unusual behavior observed in the optoelectronic data has been attributed to dynamical electron-hole correlations,[24] carrier localization,[22] carrier interactions with varying magnetic moments,[23] etc.

The figure of merit is a strong function of doping and temperature T. Doping may play a significant role in enhancing thermoelectric efficiency[25] and besides, intentional doping may lead to a better understanding of the ground state properties. For example, a recent theoretical study showed that doping of Re and Ru atoms for Mn in AlMnSi C54-phase could drastically increase its ZT from 0.12 to 0.38 at 540 K.[26]

In this paper, we investigate the electronic, magnetic, optical, and thermoelectric properties of Fe_2VAl with Fe antisite defects ($Fe_{2+x}V_{1-x}Al$) as obtained from the modern band structure computations with the recently developed Tran and Blaha modified Becke-Johnson potential functional (denoted as TB-mBJ).[27,28] The TB-mBJ functional yields band gaps in good agreement with experiment[29–32] in contrast to the local density approximation (LDA) or the generalized gradient approximation (GGA) functionals. Hence, enables direct, quantitative comparisons of optoelectronic properties with experiment, without any adjustments, such as scaling the magnitude of the absorption or applying scissors operators to fix the gap. We extensively discuss the results in relation to experimental data. We hope that they will motivate future experimental investigations of the band structure of Fe_2VAl, particularly using parallel measurement techniques.

II. COMPUTATIONAL DETAILS

The primitive cell of full-Heusler alloy Fe_2VAl ($L2_1$ structure, space group $Fm3m$) contains four atoms forming a lattice with the Wyckoff positions Fe1(1/4,1/4,1/4), Fe2(3/4,3/4,3/4), V(1/2,1/2,1/2), and Al(0,0,0). The Fe antisites are modeled via supercell of varying Fe-defect compositions, x=0.25, 0.50, 0.75, and 1.00 with the space group $Pm3m$, $P4/mmm$, $Pm3m$, and $Fm3m$, respectively (c.f. Fig. 1). The experimental lattice parameter, a = 5.76 Å for the parent Fe_2VAl material[33] is used as an initial value for the ground-state structure optimization using the GGA functional in the Perdew-Burke-Ernzerhof version.[58]

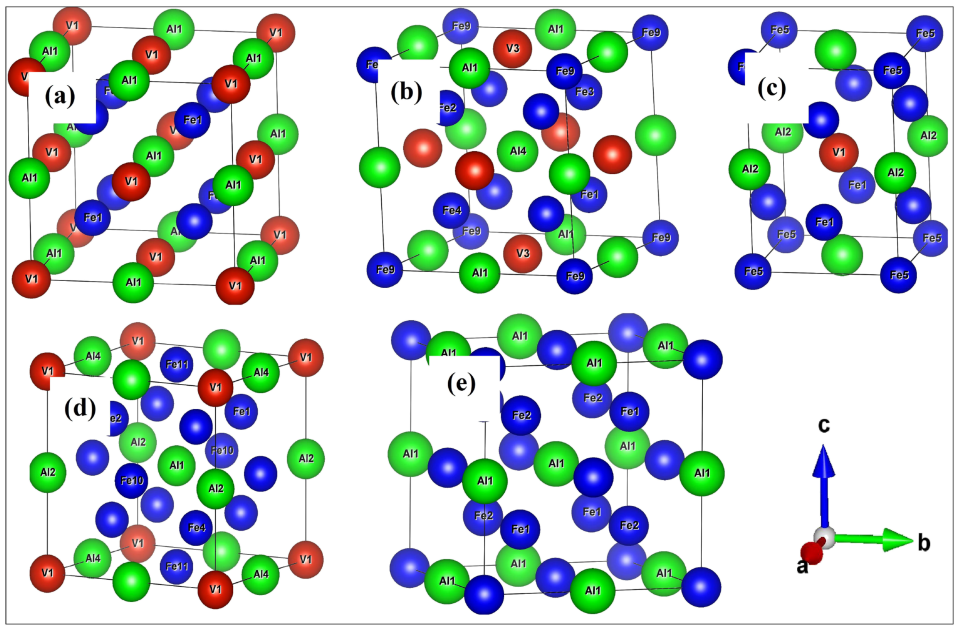

FIG. 1. The unit cell structures of $Fe_{2+x}V_{1-x}Al$ with different compositions (a) x = 0.00, $Fm3m$ (b) x = 0.25, $Pm3m$ (c) x = 0.50, $P4/mmm$ (d) x = 0.75, $Pm3m$ and (e) x = 1.00, $Fm3m$.

Aside from using the TB-mBJ potential, other details of our calculations are standard. Unless otherwise stated, the results presented below are obtained using the TB-mBJ potential. Herein, we obtain the single-particle properties with density functional theory[34,35] calculations using the full potential linearized augmented plane wave (LAPW) method, as implemented in WIEN2K.[36] We utilized well-converged basis sets with dense Brillouin zone sampling, which are essential for the optical properties. The LAPW sphere radii were 2.34, 2.34, and 2.20 Bohr for Fe, V, and Al atoms. Thermoelectric properties were obtained using the BoltzTraP package.[37] The Fermi level at zero temperature is taken as the chemical potential in the transport calculation.

III. RESULT AND DISCUSSION

A. Electronic properties

We begin the discussion of our results with the electronic structure of the parent Fe_2VAl. The density of states (DOS) and the spectra are shown in Fig. 2. The band structure is qualitatively similar to those previously reported,[23,24] but quantitative differences result from the use of the TB-mBJ functional, and these are important. Unlike the GGA results, which predict a nonmagnetic semimetal solution, the results obtained using the TB-mBJ led to the opening of an indirect energy gap, $E_g \approx 0.22$ eV along the $\Gamma - X$ of the high symmetry of the Brillouin zone in agreement with experiment.[21,38] Blic *et al*[19] using a Hybrid functional reported a higher $E_g \sim 0.34$ eV. Our calculations show that the conduction band maximum (CBM) is mainly dominated by V d-states whereas the valence band maxima (VBM) is formed primarily by the Fe d-t_{2g} states. This scenario suggests that the E_g are formed by $d - d$ interactions. Surprisingly, the TB-mBJ results are in good agreement with experiments[21,38] while the DFT plus effective Coulomb interaction calculations (not shown) led to a magnetic metallic solution.

Iron antisite introduces some fluctuations in the local environment resulting in a disordered material. To explore this, we systematically incorporate Fe antisites of concentration, x in $Fe_{2+x}V_{1-x}Al$, where $0 < x \leq 1.0$. The unit cell of $Fe_{2+x}V_{1-x}Al$ contains two inequivalent Fe-sites: Fe1 and Fe2. Our simulations show that there are structural phase transitions as Fe antisite concentration is varied between $0 < x \leq 1.0$. For x=0 (Fe_2VAl) Fe1 is occupied by V and Fe2 by Fe, where Fe in Fe2-site is magnetically inactive. Fe1-site is coordinated by eight transition metal atoms (Fe2,V) and has no Al neighbors. The Fe2-site is coordinated by four Al atoms and four Fe1 atoms. With increasing Fe concentration, the parent cubic structure (space group $Fm3m$) transits to the high pressure cubic polymorph (space group $Pm3m$) at $x \approx 0.25$ before undergoing structural phase transition to a tetragonal polymorph around $x \approx 0.50$ and then transiting back to the cubic structure (space group $Fm3m$) for $x > 0.50$ (cf. Fig. 1). To better understand the origin of the structural phase transition, we further explore the electronic structure. With increasing Fe antisite concentration, the Fe d states splits into

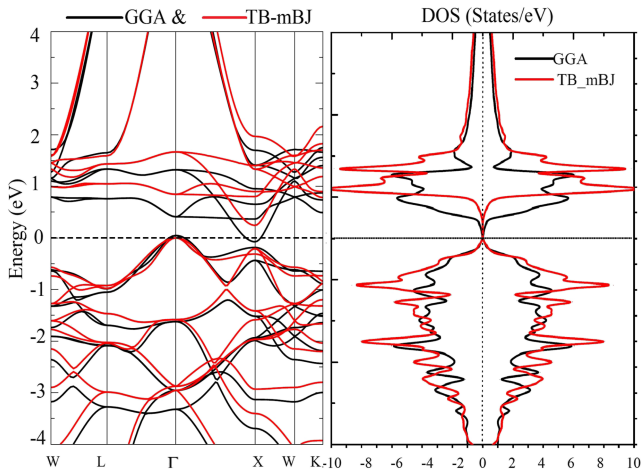

FIG. 2. The calculated band structure and total density of states of Fe_2VAl obtained using the PBE-GGA and TB-mBJ.

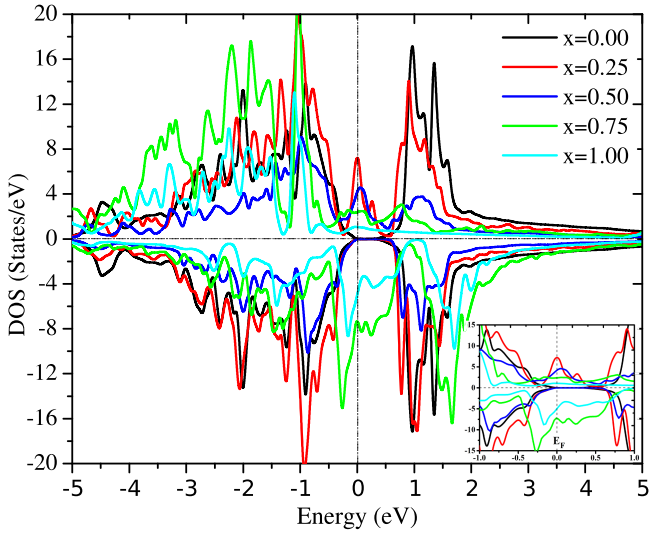

FIG. 3. The total density of states of $Fe_{2+x}V_{1-x}Al$ obtained using the TB-mBJ potential functional (inset:DOS around the E_F).

bonding (e_g) and antibonding (t_{2g}) states, which enhances the formation of a band gap in at least one of the spin channels due to the Fe-Fe hybridization.[7] From the total DOS (Fig. 3), we further confirm the ferromagnetic, half-metalicity observed in the dispersion for $x \approx$ 0.25-0.5, where the spin-down channel show semiconductor character and a metallic behavior in the spin-up channel due to the formation of a peak mainly from the Fe- and V-d states at the Fermi level (E_F). Our finding is consistent with some experimental results,[13,14] which show that Fe-rich $Fe_{2+x}V_{1-x}Al$ can have a giant magnetoresistance. From our results, we infer that the highest magnetic moment is obtained for $x \sim 0.75$ and the Fe d peaks are dispersed in both the two spin channels, indicating a metallic solution (c.f. Fig 3), which persists through to $x = 1$ (Fe_3Al).

The Fe antisites also enhance the magnetic properties. We find a ferromagnetic, ordered state in the range $x = 0.25 - 1.00$. For $x = 0.25$, the partial moments obtained using the TB-mBJ potential are 0.13, 2.68, and -0.13 μ_B for Fe1, Fe2, and V, respectively, with a total magnetic moment of $\approx 3.0\ \mu_B$ (c.f. Table I). The total magnetic moment value is consistent with the 2.2-3.2 μ_B obtained using the Green function based Koringa-Kohn-Rostoker calculations.[39] With increasing Fe concentration, the Fe1 moments increase linearly, whereas that of Fe2 site slightly decrease after $x \geq 0.50$ (cf. Table I). We attribute this scenario to be due to to the magnetically active Fe1 sites that in turn polarize Fe2 atoms. The V-site magnetic moment is a small negative contribution as the compound is now a feeble ferrimagnetic rather than a broad ferromagnet. For $x = 1$ (Fe_3Al) the calculated local magnetic moment for the Fe atom in Fe1 site is 2.08 μ_B, which agrees well with the experimental value of 2.14 μ_B from polarized neutron diffraction method[40] and 2.42 μ_B from DC magnetometer with SQUID sensor measurement.[41] Our results are also consistent with the previous theoretical results of $\approx$2.2 μ_B.[23,42]

TABLE I. The total and partial moments (μ_B) of $Fe_{2+x}V_{1-x}Al$ obtained using the PBE-GGA and TB-mBJ potential functionals.

	GGA				TB-mBJ			
x	Fe1	Fe2	V	Total	Fe1	Fe2	V	Total
0.00	0.000	0.007	–0.014	0.007	0.000	0.007	–0.014	0.007
0.25	0.126	2.532	–0.116	3.000	0.126	2.682	–0.129	3.000
0.50	1.109	2.593	–0.814	5.781	1.177	2.673	–0.871	5.978
0.75	1.583	2.499	–0.998	18.038	1.876	2.572	–1.199	19.530
1.00	1.917	2.421	0.000	5.947	2.082	2.498	0.000	6.173

B. Optical and transport properties

Optical spectroscopy, while less direct than angle-resolved photoemission experiments, provides detailed information about the electronic structure and has the advantage of being a true bulk probe. There have been some optical studies of FeVAl-family.[13,43–49] Herein, we study the optical spectra of $Fe_{2+x}V_{1-x}Al$ obtained using the TB-mBJ potential. While it is conventional to plot calculated optical data with a broadening added to mimic experimental data, we instead show results with practically no broadening to show more clearly the features in the calculated spectra. The calculated optical properties are shown in Fig. 4. Experimental data show that the reflectivity, R(E) increases with increasing Fe concentration in the low energy region especially as $R(E \rightarrow 0)$.[13] Our simulations support this observation [c.f. Fig. 4(a)] except at very large Fe concentration where the magnitude of $R(0)|_{x=0.75}$ is slightly greater than that of $R(0)|_{x=1.0}$. We attribute this discrepancy to the DFT calculations carried out at zero temperature as compared to the experimental measurement, which was done at room temperature. The experimental optical spectra in the infrared region show two prominent peaks attributed to optical phonon and a Drude continuum peak (see, e.g., Fig.2 of Ref. 14), which increases in magnitude as Fe concentration increases. These peaks are missing in our result because the corresponding interactions are not included in our calculation. However, in the visible light region, our calculations show that the prominent optical conductivity peak around energy, $E \approx 2.0$ eV decreases as $x \rightarrow 1.0$ in good agreement with experimental data.[14]

The thermoelectric applicability of materials depends very sensitively on the Seebeck coefficient S and the electrical conductivity σ, which is encoded in a dimensionless quantity, the figure of merit ZT. Therefore, an efficient thermoelectric material is characterized by a high value of S and σ with a low value of κ,[50] so as to have a ZT value about or greater than unity. Because these three quantities are strongly correlated, it has been a challenge on how to increase ZT to value for practical applications for most materials. The low efficiency of energy conversion is a major mitigating factor for practical applications of thermoelectric materials as a power generator. Typical thermoelectric materials like Tellurium, Lead, Antimony, and Selenium are considered to be more efficient; unfortunately, they are toxic, hence degrading to the environment.[51] A consequence of these, search for new, low-cost and environmentally-friendly materials with high values of ZT is of great interest, with diverse potential technological applications.

To better characterize the thermoelectric properties of $Fe_{2+x}V_{1-x}Al$, we calculate Seebeck coefficient S, electronic thermal conductivity κ/τ, electrical conductivity σ/τ, and then the figure of merit. Figure 5 show the thermoelectric quantities for various concentrations of Fe antisite. The Seebeck coefficient S is a sensitive test of the electronic structure of metals in the vicinity of the Fermi level. With the Fe defects, S values are found to saturate at ~350 K.[52] Our calculations show a similar trend. We observe a linear behavior up to 200 K, and then, it stabilizes at ~300 K except for $x = 1.0$ [cf. Fig. 5(a)]. Similar temperature trend was reported for $Fe_2V_{1+y}Al_{1-y}$ $(0 \leq y \leq 0.12)$ compounds.[53] Observe that the value of S is negative for the entire temperature range except for $x = 0.25$, which is a

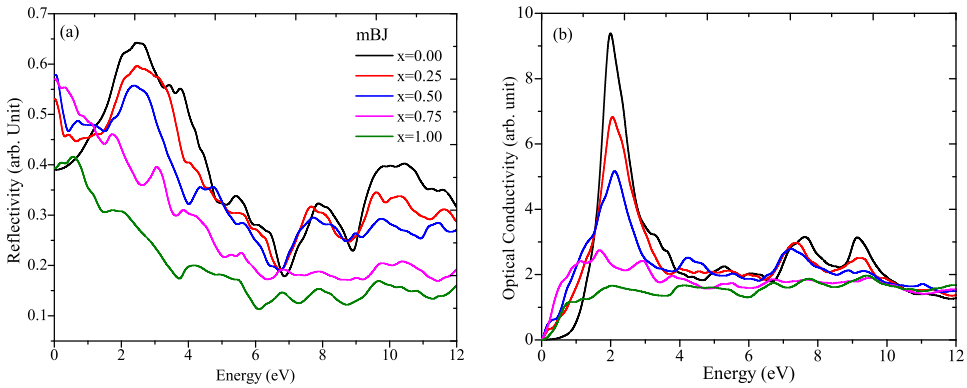

FIG. 4. The evolution of the (a) Reflectivity and (b) optical conductivity of $Fe_{2+x}V_{1-x}Al$ due to Fe antisite concentration obtained using the TB-mBJ potential functional.

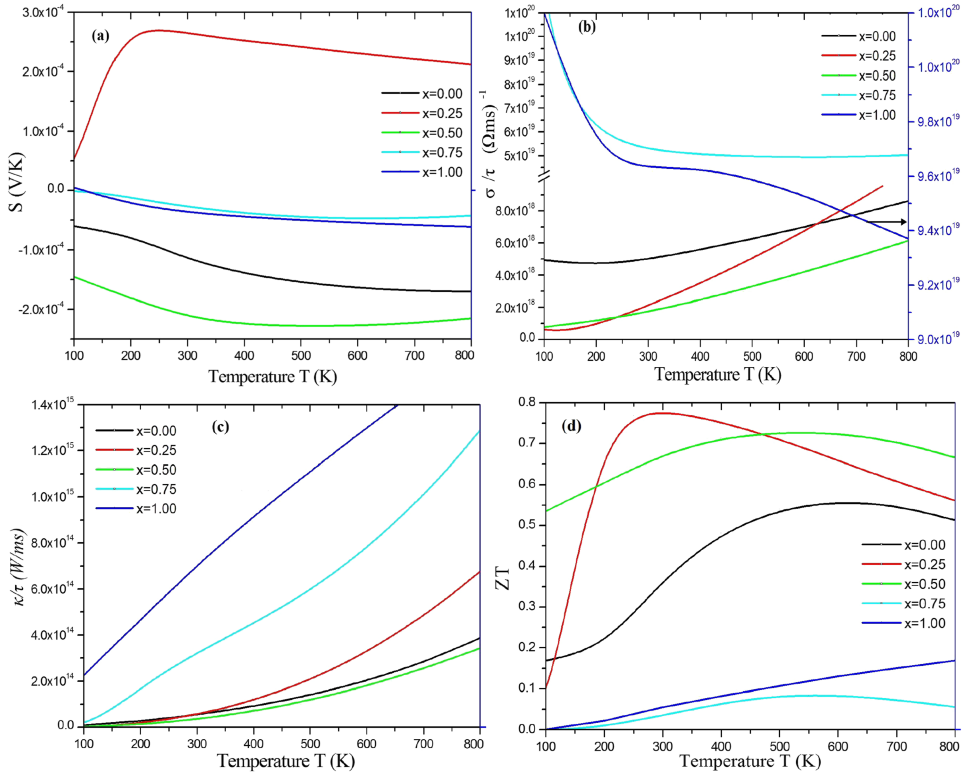

FIG. 5. The thermoelectric properties of $Fe_{2+x}V_{1-x}Al$ as functions of temperature for various Fe antisite concentration obtained using the TB-mBJ potential functional: (a) Seebeck coefficient, (b) Electrical conductivity (blue line represents $x = 1.0$, scaling on the right vertical axis), (c) Thermal conductivity, and (d) Figure of merit ZT.

fingerprint of N-type charge carriers. Since S is a measure of the voltage produced by a temperature gradient in the material, linear temperature dependence at low temperature is a signature of a potential promise for thermoelectric device applications.[54] Experimental data of the Seebeck coefficient are available only for x=0.0 between -120 and -130 μV/K at room temperature. Our result of -150 μV/K at 300 K is in good agreement with the experimental data.[55]

To further investigate the observed thermopower, we calculated the electrical conductivity (σ/τ) as a function of temperature [c.f. Fig. 5(b)]. As it is evident from the plots, (σ/τ) decreases from ~50 K, forming a valley around 150 K, and then increases slowly for $0 \leq x \leq 0.50$. The valley represents a peak in the electrical resistivity curve. The slow increase after the valley indicates a negative slope of the resistance, which signifies a semiconductor-like behavior. Similar effect can be compared with the variation of temperature dependence of electrical resistivity [cf. Fig.2 of Ref. 52]. On the other hand, there is a sharp decrease of (σ/τ) up to 300 K and a slow decline for $0.75 \leq x \leq 1.00$ confirming the metallic behavior observed in the electronic structure in this concentration. One may also calculate an independent electrical conductivity (σ) if the charge relaxation time, τ is known. The room temperature value of (σ/τ) obtained from Fig. 5(a) is around $5\text{x}10^{18}$ $(\Omega ms)^{-1}$ for $x = 0.0$. The experimental resistivity, $\rho \sim 0.75$ $m\Omega cm$ (300 K)[56] yields a τ value of $\sim 2.10 \times 10^{-14}$ s, being higher than the 0.90×10^{-14}s (GGA) and 1.4×10^{-14}s (B1–WC).[19] While using a τ value of 2.10×10^{-14}s and (σ/τ) as 5×10^{18} $(\Omega ms)^{-1}$, the calculated resistivity of Fe_2VAl is 0.95 $(m\Omega cm)$ at 300 K, which is in close agreement with the experimental one.[56] The calculated charge concentration in Fe_2VAl is 3.05×10^{20} cm^{-3}, is consistent with the experimental value of 3.7×10^{20} cm^{-3} [22] but smaller than the 4.8×10^{20} cm^{-3} obtained from a Hall effect study at 300 K.[55] Since τ is generally difficult to systematically compute and for x=0.25, 0.50, 0.75, and 1.00 are yet unknown at least from experiment, we cannot unambiguously determined the resistivity. However, from Fig. 5(b) we can estimate that the resistivity for x=0.75 and 1.00 is lower than that for x=0.0, 0.25 and 0.50 at room temperature.

The thermal conductivity as a function of temperature is shown in Fig. 5(c). It increases with the temperature in all cases. The thermal conductivity for $x = 1.0$, however, shows a linear dependence with temperature because the increasing temperature leads to the increment in the number of charge carriers due to the metallic nature. The nonlinear variation of thermal conductivity at the low-temperature range has an onset value at 50 K for x = 0.0, 0.25 and 0.50, a signature of a semiconductor-like behavior for the down-spin electrons.

Using S, σ/τ, and κ/τ, we calculate the ZT profile as a function of increasing temperature for various Fe antisite concentrations as shown in Fig. 5(d). The calculated ZT surprisingly show its highest value around the room temperature ~ 300 K. At 300 K, we can obtain the numerical values of ZT as 0.30, 0.75, 0.65, 0.05, and 0.05 for x=0.0, 0.25, 0.50, 0.75, and 1.0, respectively. The most efficient thermoelectric materials such as Bi_2Te_3, PbTe, and Bi_2Se_3 show ZT values of 0.85-1.20.[57] The recent advancement by doping thallium impurity in PbTe results in an increased ZT value above 1.50 at 773 K.[50] The $Fe_{2+x}V_{1-x}Al$ with antisite doping of 0.25 show the highest ZT value of ≈ 1 at 300 K, much higher than that of other Fe-based Heusler compounds. While this is significant, the calculated ZT is still not enough for practical applications of $Fe_{2+x}V_{1-x}Al$ as a thermoelectric device (note that the present value may also somewhat overestimated since the lattice thermal conductivity is not taken into account). It, however, shows a promise that with a better choice of doping element (probably heavy elements), the enhancing thermoelectric efficiency of $Fe_{2+x}V_{1-x}Al$ may be further increased to a point where their technological applications become possible.

IV. CONCLUSION

The electronic, magnetic, and optical properties of $Fe_{2+x}V_{1-x}Al$ have been investigated using first-principles electronic structure and transport calculations. We find rather rich and multifunctional properties ranging from ferromagnetic metal, half-metalicity, and promising thermopower properties for $Fe_{2+x}V_{1-x}Al$. For Fe antisite, x=0.0, we predict in good agreement with experiments, the semiconducting behavior with a band gap ~0.22 eV. For $0.25 \leq x \leq 0.50$, the material is found to be a ferromagnetic, half-metal. The estimated integer values of the magnetic moment are in agreement with the half-metallic ground state. For x=0.75 and 1.0, a true metallic character is observed. The calculated optical spectra agree well with the experimental ones in the UV-VIS energy range. The predicted high ZT value ~ 0.75 for x=0.25, is a fingerprint that $Fe_{2+x}V_{1-x}Al$ is promising for thermoelectric device applications especially as it is low-cost and environmentally-friendly.

[1] Z. H. Liu, H. N. Hu, G. D. Liu, Y. T. Cui, J. L. C. M. Zhang, and G. Wu, Phys. Rev. B **69**, 134415 (2004).
[2] K. Yamauchi, B. Sanyal, and S. Picozzi, Appl. Phys. Lett. **91**, 69062506 (2007).
[3] D. P. Rai, Sandeep, A. Shankar, M. P. Ghimire, A. P. Sakhya, T. P. Sinha, and R. K. Thapa, Materials Research Express **3**, 075022 (2016).
[4] D. P. Rai, D. T. Khating, P. K. Patra, S. J. Hashemifar, M. Jamal, Lalmuanpuia, M. P. Ghimire, Sandeep, Rosangliana, and R. K. Thapa, Indian Journal of Physics **84**, 593 (2010).
[5] K. L. Kobayashi, H. S. T. Kimura, K. Terakura, and Y. Tokura, Nature **395**, 677 (1998).
[6] A. Fert, Rev. Mod. Phys. **80**, 1517 (2008).
[7] I. Galanakis and P. Mavropoulos, Phys. Rev. B **67**, 104417 (2003).
[8] K. Schwarz, J. Phys. F Met. Phys. **16**, L211 (1986).
[9] W. C. Kim, K. Kawaguchi, N. Koshizaki, M. Shoma, and T. Matsumoto, J. Appl. Phys. **93**, 8032 (2003).
[10] Y. K. Kuo, K. M. Sivakumar, and H. Chen, Phys. Rev. B (2005).
[11] K. H. J. Buschow and P. van Engen, J. Magn. Magn. Mater. **25**, 90 (1981).
[12] Y. V. Kudryavtsev, Y. P. Lee, and J. Y. Rhee, Phys. Rev. B **66**, 115114 (2002).
[13] H. Okamura, J. Kawahara, T. Nanba, S. Kimura, K. Soda, U. Mizutani, Y. Nishino, M. Kato, I. Shimoyama, H. Miura *et al.*, Phys. Rev. Lett. **84**, 3674 (2000).
[14] T. Naka, K. Sato, M. Taguchi, T. Nakane, F. Ishikawa, Y. Yamada, Y. Takaesu, T. Nakama, and A. Matsushita, Phys. Rev. B **85**, 085130 (2012).
[15] J. Herfort, H. P. Schonherr, and K. H. Ploog, Appl. Phys. Lett. **83**, 3912 (2003).
[16] S. Wurmehl, G. H. Fecher, H. C. Kandpal, V. Ksenofontov, C. Felser, and H. J. Lin, Appl. Phys. Lett. (2006).
[17] K. Renard, A. Mori, Y. Yamada, S. Tanaka, H. Miyazaki, and Y. Nishino, J. Appl. Phys. **115**, 033707 (2014).
[18] M. Mikami, Y. Kinemuchi, K. Ozaki, Y. Terazawa, and T. Takeuchi, J. Appl. Phys. **111**, 093710 (2012).
[19] D. I. Blic and P. Ghosez, Phys. Rev. B **83**, 205204 (2011).
[20] Y. Nishino, M. Kato, S. Asano, K. Soda, M. Hayasaki, and U. Mizutani, Phys. Rev. Lett. **79**, 1909 (1997).
[21] C. S. Lue, J. H. Ross, Jr., C. F. Chang, and H. D. Yang, Phys. Rev. B **60**, R13941 (1999).
[22] G. Y. Guo, G. A. Botton, and Y. Nishino, J. Phys. Condens. Matter **10**, L119 (1998).

[23] D. J. Singh and I. Mazin, Phys. Rev. B **57**, 14352 (1998).
[24] W. Ruben and W. E. Picket, Phys. Rev. B **58**, 6855 (1998).
[25] A. Matsushita, T. Naka, Y. Takano, T. Takeuchi, T. Shishido, and Y. Yamada, Phys. Rev. B **65**, 075204 (2002).
[26] A. Yamamoto, H. Miyazaki, and T. Takeuchi, J. Appl. Phys. **115**, 023708 (2014).
[27] F. Tran and P. Blaha, Phys. Rev. Lett. **102**, 226401 (2009).
[28] A. D. Becke and M. R. Roussel, Phys. Rev. A **39**, 3761 (1989).
[29] C. E. Ekuma, D. J. Singh, J. Moreno, and M. Jarrell, Phys. Rev. B **85**, 085205 (2012).
[30] D. J. Singh, Phys. Rev. B **82**, 205102 (2010).
[31] D. J. Singh, Phys. Rev. B **82**, 155145 (2010).
[32] D. P. Rai, J. Maibam, B. I. Sharma, A. Shankar, R. K. Thapa, and S. H. Ke, J. Alloys Compd. **589**, 553 (2014).
[33] E. Shreder, S. V. Streltsov, A. Svyazhin, A. Makhnev, V. V. Marchenkov, A. Lukoyanov, and H. W. Weber, J. Phys. Condens. Matter **20**, 045212 (2008).
[34] P. Hohenberg and W. Kohn, Phys. Rev. **136**, B864 (1964).
[35] W. Kohn and L. J. Sham, Phys. Rev. **140**, A1133 (1965).
[36] P. Blaha, K. Schwarz, G. K. H. Madsen, D. Kvasnicka, J. Luitz, and K. Schwarz, An Augmented Plane Wave plus Local Orbitals Program for Calculating Crystal Properties. Wien2K Users Guide, Techn. Universitat Wien, Wien (Cambridge University Press, 2008).
[37] G. K. H. Madsen and D. Singh, Comput. Phys. Commun. **175**, 67 (2006).
[38] C. S. Lue and J. H. Ross, Phys. Rev. B **61**, 9863 (2000).
[39] A. Bansil, S. Kaprzyk, P. E. Mijnarends, and J. Tobol, Phys. Rev. B **60**, 13396 (1999).
[40] S. J. Pickart and R. Nathans, J. Appl. Phys. **31**, S372 (1960).
[41] A. A. Coelho, M. Imaizumi, B. Laks, A. Araujo, M. Mota, S. Gama, M. Jafelicci, and L. C. Varanda, J. Magn. Magn. Mater. **272-276**, 769–770 (2004).
[42] K. Bose, V. Drchal, J. Kudrnovsky, O. Jepsen, and O. K. Andersen, Phys. Rev. B **55**, 8184 (1997).
[43] L. S. Hsu, Y. K. Wang, G. Y. Guo, and C. S. Lue, Phys. Rev. B **66**, 205203 (2002).
[44] V. Sharma and G. Pilani, J. Magn. Magn. Mater. **339**, 142–150 (2013).
[45] J. Y. Rhee, J. Korean. Soc. **63**, 1975–1979 (2013).
[46] B. Xu, J. Liu, and L. Yi, Phys. Lett. A **363**, 312–316 (2007).
[47] Y. Feng, J. Y. Rhee, T. A. Wiener, and L. L. Miller, Phys. Rev. B **63**, 165109 (2001).
[48] F. Wooten, *Optical Properties of Solids* (Academic Press, New York, 1972).
[49] M. Kumar, T. Nautiyal, and S. Auluck, J. Phys.: Condens. Matter **21**, 446001 (2009).
[50] J. P. Heremans, V. Jovovic, E. S. Toberer, A. Saramat, K. Kurosaki, A. Charoenphakdee, S. Yamanaka, and G. J. Snyder, Science **321**, 554 (2008).
[51] G. E. Smith and R. Wolfe, J. Appl Phys. **33**, 841 (1962).
[52] Y. Nishino, S. Deguchi, and U. Mizutani, Phys. Rev. B (2006).
[53] H. Miyazaki, S. Tanaka, N. Ide, and Y. Nishino, Mater. Res. Express **1**, 015901 (2014).
[54] V. Sharma, A. K. Solanki, and A. Kashyap, J. Magn. Magn. Mater. **322**, 2922 (2010).
[55] M. Kato and Y. Nishino, Proceedings XVI ICT 5-8, May (1997).
[56] M. Vasundhara, V. Srinivas, and V. V. Rao, Phys. Rev. B **77**, 224415 (2008).
[57] D. Y. Chung, T. Hogan, J. Schindler, L. Iordarridis, P. Brazis, C. R. Kannewurf, C. Baoxing, and C. Uher, Proceedings XVI ICT 5–8, May, 1997.
[58] J. P. Perdew, K. Burke, and M. Ernzerhof, Phys. Rev. Lett. **77**, 3865 (1996).